AIAA JOURNAL
Vol. 41, No. 10, October 2003

Adaptivity, Sensitivity, and Uncertainty: Toward Standards of Good Practice in Computational Fluid Dynamics

D. Pelletier,* É. Turgeon,† and D. Lacasse†
École Polytechnique de Montréal, Montréal, Québec H3C 3A7, Canada
and
J. Borggaard‡
Virginia Polytechnic Institute and State University, Blacksburg, Virginia 24061

Three issues related to good computational fluid dynamics (CFD) practice are discussed. First, adaptive methods are shown to be a simple tool to perform systematic grid refinement studies needed to achieve solutions with controlled accuracy (verification of simulations). Second, it is shown that the sensitivity equation method provides insights about which parameters critically affect the flow response. Finally, flow sensitivities are used to propagate model parameter uncertainties through the CFD code to yield uncertainty estimates of the CFD predictions. This provides a rigorous framework for comparing predictions to measurements (validation of predictions). These combined approaches help to build confidence in CFD predictions and develop good CFD practice. The resulting uncertainty bars put CFD on par with experimental techniques. The approaches are demonstrated on two-dimensional problems: a k–ϵ model of the flow in an annular turn-around duct and conjugate free convection with variable fluid properties. Taken together, these approaches offer a good prospect for developing families of computing methods that can be viewed as standards of good practice in CFD, ensuring that verification and validation studies are performed on solid grounds.

Introduction

ACCURATE and reliable prediction of fluid flows has preoccupied the computational fluid dynamics (CFD) community over the past several years. A review of the literature reveals that, in many cases, predictions of a given flow by different authors show unexpectedly large scatter. This can be especially disconcerting when people produce vastly different predictions while using similar models and numerical methods. For example, Table 1 presents the predicted length of the recirculation zone for turbulent flow over a backward-facing step.[1] All authors use a variant of the k–ϵ model with wall functions and a TEACH-type solution algorithm.[1] The only exceptions are the prediction of Donaldson, who used a Reynolds stress model (RSM) and that of Ilinca et al. obtained with an adaptive finite element method. In this case, the only possible causes for the differences observed between authors are the meshes used, as well as details of the computer implementation of the algorithm, because the authors use the same boundary conditions (or claim to do so). Unfortunately, the techniques for computing the reattachement length can not be assessed from the cited references.[1]

This is a good example illustrating the need for a uniform way of performing CFD simulations and of reporting their results. Note that the experimentally measured length of the recirculation zone is reported with an uncertainty interval accounting for uncertainties due to both the operating conditions and the experimental equipment. This is not the case for CFD results that are reported as a single number and that provide no clues about the results' numerical accuracy. Moreover, reported results provide no clues as to the effect of uncertainties in the data input to the flow solvers: boundary conditions that are guessed or inaccurate, uncertainties in constitutive relations for physical properties, etc. Hence, there is a need to quantify the numerical accuracy of flow solvers, to assess the relative importance of various parameters controlling the flow, and to estimate the uncertainty of the flow response due to uncertainties in the input parameters. Finally, there is a need for some form of guidelines to perform these separate tasks satisfactorily.

The present paper illustrates how numerical errors can be controlled via mesh adaptation to provide solutions of high quality and accuracy. It also shows how sensitivity analysis can yield uncertainty estimates of the flow response to uncertainties or inaccuracies in the flow solver input data. The former provides a tool for assessing to what extent the differential equation have been solved exactly. The latter provides a tool to assess to what extent these accurate solutions can be trusted. The larger the uncertainty of the flow response, the lower the confidence.

The present paper should be viewed in the light of efforts on verification and validation as discussed by Roache[2] and in Ref. 3. Both define verification as a synonym for solving the equations accurately, that is, solving the equations right. Hence, verification consists of a mathematical and numerical analysis exercise. Validation is defined a process to determine whether the right equations are solved for the process at hand, that is, solving the right equations. It is essentially an engineering activity involving comparison with laboratory or field data. Here, we provide one additional step: Sensitivity analysis is used to provide uncertainty intervals for the CFD solution computed at the nominal values of the parameters.

The paper is organized as follows. First, we present a brief discussion of various sources of errors and uncertainty. We then present an example of verification and validation of CFD simulations of turbulent flow in an annular turn-around duct. Emphasis is on good CFD practice for assessing grid convergence of predictions and the effects of input parameters on the CFD predictions, namely, data in wall functions and inflow boundary conditions. This is followed by a discussion of the sensitivity equation method. Free convection of corn syrup is used as an example because uncertainties with regard to several parameters are reported by the experimentalists. Sensitivity analysis on four parameters is used to compute uncertainty intervals

Received 20 November 2001; revision received 18 February 2003; accepted for publication 21 February 2003.

*Canada Research Chair, Département de Génie Mécanique. Associate Fellow AIAA.

†Graduate Student, Département de Génie Mécanique; currently Senior Computing Analyst, Multi-Disciplinary Computing Methods, (OISR4), Pratt and Whitney Canada, 1000, Marie-Victorin, Longueuil, Québec J4G 1A1, Canada.

‡Associate Professor, Department of Mathematics. Senior Member AIAA.

Table 1 Flow over a backward-facing step

Author(s)	Turbulence model	L/H
Kim et al.[1]	Experiment	7 ± 0.5
Mansour and Morel[1]	k–ϵ	5.2
Pollard[1]	k–ϵ	5.88
Rodi et al.[1]	k–ϵ	5.8
Launder et al.[1]	Algebraic stress model	6.9
Abdelmeguid et al.[1]	k–ϵ	6
Demirdzic et al.[1]	Modified k–ϵ	6.2
Donaldson et al.[1]	RSM	6.1
Ilegbusi and Spalding[1]	Modified k–ϵ	7.2
Nallasamy and Chen[1]	k–ϵ	5.8
Syed et al.[1]	k–ϵ	5.8
Ilinca et al.[7]	k–ϵ	6.2

of the CFD predictions, which are compared with measurements. The paper ends with conclusions.

Sources of Errors and Uncertainty

One cannot discuss accuracy and errors without discussing the sources of errors in a CFD simulation. Oberkampf et al. provide a proper taxonomy of errors[4]: physical modeling errors, discretization errors, programming errors, and computer roundoff errors. Programming errors are mistakes that are beyond the scope of the present paper. Computer roundoff errors are not considered here. Thus, we are left with physical modeling errors and discretization errors. According to Roache,[2] discretization errors can be evaluated by grid refinement (verification) studies, whereas modeling errors can only be assessed by validation against measurements.

Errors include 1) the choice of polynomial interpolation function for finite element approximations, or for flux evaluation in finite volume methods; 2) the discretization (meshing) of the domain; 3) the representation or interpolation of boundary conditions; 4) the discretization of curved geometries; 5) the discretization of data such as temperature-dependent fluid properties or the eddy viscosity; 6) the convergence tolerance of linear and nonlinear equation solvers, and 7) the nonlinear mixed boundary conditions such as wall functions. All of these aspects are within the control of the analyst: Grid refinement studies can be performed, the grid convergence index can be computed to assess accuracy,[2] error estimates can be obtained, and iterative tolerances can be varied to assess their impact on overall accuracy. Adaptive methods are an especially good tool for assessment and control of these errors, that is, when a given simulation is verified.

As mentioned earlier, modeling errors can only be assessed by comparison of verified predictions with measurements. To make this exercise meaningful, one must account for uncertainties in both the measurements and the input parameters to the flow solver. All such input parameters are prescribed to a certain level of accuracy or uncertainty that has a direct impact on the accuracy/uncertainty of the CFD solution. For example, a correlation of viscosity as a function of temperature may be accurate to say 6% (Ref. 5), whereas an angle of attack might be measured to within, for example, 0.1 deg. Finally, manufacturing tolerances result in uncertainties in the geometrical data. All of these uncertainties are beyond the control of the analyst. Yet they must be accounted for to achieve meaningful comparisons with measurements. Sensitivity analysis can be used to derive uncertainty bars for CFD predictions, provided that parameter uncertainties are small compared to the nominal values of the parameters.

Turbulent Flow

This section describes the use of an adaptive finite element method to produce accurate (verified) solutions of the Reynolds-averaged Navier–Stokes equations by the use of the standard k–ϵ model of turbulence with wall functions. Here, the emphasis is on the use of adaptivity to perform systematic and rigorous grid refinement studies to monitor grid convergence of all important aspects of the solution. This includes grid convergence of nonlinear boundary conditions such as wall functions. Such aspects are rarely reported in the literature, yet they are crucial to good CFD practice.

Model Problem

The problems of interest are modeled by the time-averaged continuity and momentum equations:

$$\nabla \cdot \boldsymbol{u} = 0 \tag{1}$$

$$\rho \boldsymbol{u} \cdot \nabla \boldsymbol{u} = -\nabla p + \nabla \cdot \left[(\mu + \mu_t)(\nabla \boldsymbol{u} + \nabla \boldsymbol{u}^T) \right] \tag{2}$$

where ρ is the density, $\boldsymbol{u}$ the velocity, p the pressure, μ the viscosity, and μ_t the eddy viscosity.

This system of equations is closed with the k–ϵ model of turbulence,[6] for which the eddy viscosity is expressed in terms of two turbulence variables: the turbulence kinetic energy (TKE) k and its rate of dissipation ϵ,

$$\mu_t = \rho C_\mu (k^2/\epsilon) \tag{3}$$

The turbulence variables are governed by the following transport equations:

$$\rho \boldsymbol{u} \cdot \nabla k = \nabla \cdot \{[\mu + (\mu_t/\sigma_k)]\nabla k\} + \mu_t P(\boldsymbol{u}) - \rho\epsilon \tag{4}$$

$$\rho \boldsymbol{u} \cdot \nabla \epsilon = \nabla \cdot \{[\mu + (\mu_t/\sigma_\epsilon)]\nabla \epsilon\} + C_1(\epsilon/k)\mu_t P(\boldsymbol{u}) - C_2 \rho(\epsilon^2/k) \tag{5}$$

with $P(\boldsymbol{u})$ defined as:

$$P(\boldsymbol{u}) = \nabla \boldsymbol{u} : (\nabla \boldsymbol{u} + \nabla \boldsymbol{u}^T)$$

The constants C_1, C_2, C_μ, σ_k, and σ_ϵ are set to the values recommended by Launder and Spalding.[6] To enhance robustness of the flow solver, the turbulence equations are written in terms of the natural logarithms of the turbulence variables,[7] by solving for $\mathcal{K} = \ln(k)$ and $\mathcal{E} = \ln(\epsilon)$. This ensures that they remain positive everywhere during the course of iterations.

Boundary conditions along solid surfaces are enforced via wall functions that provide a relationship between u, the velocity tangent to the solid wall (slip velocity), and τ_w, the wall shear stress, at a given distance y from the wall:

$$u^+ = y^+ \qquad \text{for} \qquad y^+ < y_c^+ \tag{6}$$

$$u^+ = (1/\kappa)\ln(Ey^+) \qquad \text{for} \qquad y^+ \geq y_c^+ \tag{7}$$

where κ is the von Kármán constant and E is a roughness parameter. For smooth walls, we take $\kappa = 0.42$ and $E = 9.0$. The dimensionless variables u^+ and y^+ are defined as follows:

$$u^+ = u/u_\tau \tag{8}$$

$$y^+ = y\rho u_*/\mu \tag{9}$$

The critical value y_c^+ separating the linear and logarithmic velocity profiles is approximately 10.8 (Ref. 8). The wall shear stress is given by

$$\tau_w = \rho u_\tau u_* \tag{10}$$

where u_τ is the friction velocity and u_* is a second velocity scale based on the TKE:

$$u_* = C_\mu^{\frac{1}{4}} k^{\frac{1}{2}} \tag{11}$$

The value of d, the distance between the solid wall and the computational boundary, is chosen so that d^+ lies within the range of validity of the function, which is $30 < d^+ < 300$ (Ref. 9). The normal velocity is set to zero. The k equation is solved with a zero normal derivative boundary condition ($\partial k/\partial n = 0$). Finally, the boundary condition for ϵ is given by

$$\epsilon = u_*^3 \big/ \kappa y \tag{12}$$

Wall functions are, thus, nonlinear mixed boundary conditions. Because they involve the wall shear stress, their accuracy will be mesh dependent. As will be shown, it is important to monitor grid convergence of these boundary conditions to ensure reliable and trustworthy flow predictions.

Adaptive Finite Element Solver

The equations are solved by a finite element method. Because the flows considered are highly convective, numerical oscillations may occur. This undesirable effect is mitigated by the use of one of the following stabilized formulations: Streamline Upwind,[10] SUPG,[11] or GLS.[12] The equations are discretized using the seven-node triangular element,[13] which uses an enriched quadratic velocity field, a linear discontinuous pressure, and a quadratic interpolant for the logarithms of turbulence variables. This makes the scheme second-order accurate. More details about the flow solver, its accuracy, and mesh adaptation are given by Lacasse et al.[14]

Flow in a Turn-Around Duct

This approach is used to compute the flow of air in a 180-deg turnaround duct (TAD) with an annular cross section. Simulations were performed for the two geometries shown on Fig. 1. Model 1 uses a plug flow at the inlet, whereas model 2 uses a partly developed flow at the inlet. The latter conditions are closer to those observed experimentally.[15] (See Lacasse et al.[14] for details.) The Reynolds number is equal 10^5 based on the inlet velocity and the duct height (distance between the two solid walls). At the outlet, both v and the normal traction are set to zero. Zero streamwise gradients are imposed on k and ϵ. Finally, wall functions are set with $d = 0.02$ on the outer wall.

Adaptive computations were carried out for two values of the wall distance for the inner wall ($d = 0.015$ and 0.010). A typical final adaptive mesh (cycle 7) for the latter case is shown in Fig. 2. Figure 3 presents the distributions of y^+ and the slip velocity (tangential velocity along the computational boundary) along the inner wall for each adaptive cycle. These values, which enter in the evaluation of wall functions, are strongly mesh dependent. Hence, the accuracy wall function boundary conditions must be monitored for grid independence. In the bend, grid-independent values for both y^+ and the slip velocity are obtained only on the seventh and finest mesh. Computations on a finer mesh, to confirm grid independence, could not be performed due to computer memory limitations. Significant changes occur in the solution between the initial and final meshes. Nevertheless, cycles 5–7 show a trend toward grid convergence of the boundary conditions. Hence, numerical results can be interpreted with confidence in the bend region. This mesh dependence of y^+ implies a mesh dependence of the wall function boundary condition and, hence, that, of the slip velocity. Grid convergence of such data is rarely reported in the literature. Finally, notice that separation does not occur with this computational model. This is in contradiction with experimental observations.[15]

A reduction of the distance in the wall function for the inner wall causes the flow to separate. Figure 4 presents the same data as in Fig. 3, but for a wall distance of $d = 0.01$. Once again, the solution depends strongly on the fineness of the mesh near the computational

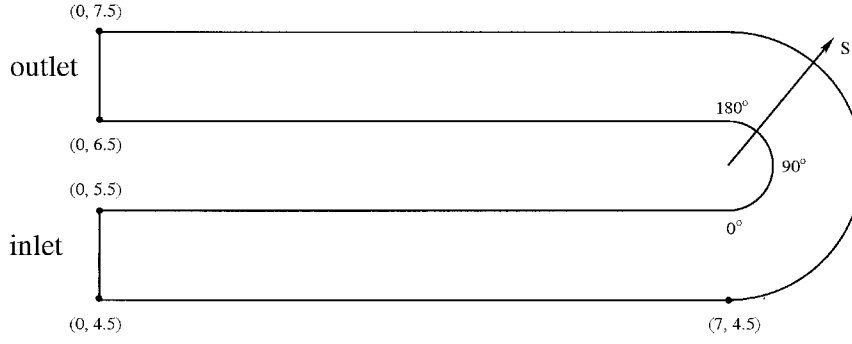

a) Computational model 1

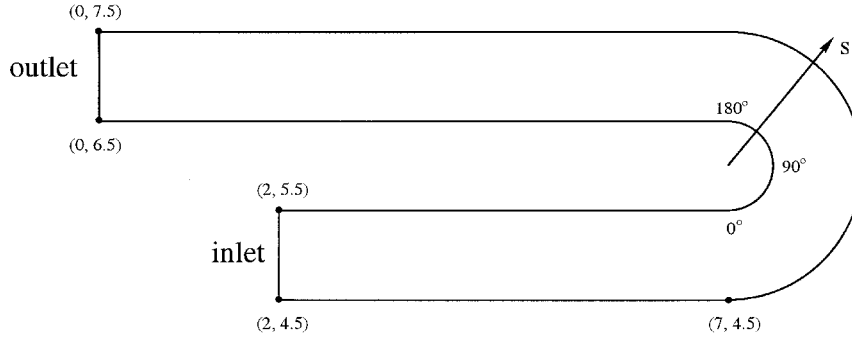

b) Computational model 2

Fig. 1 Computational models for flow in a turnaround duct.

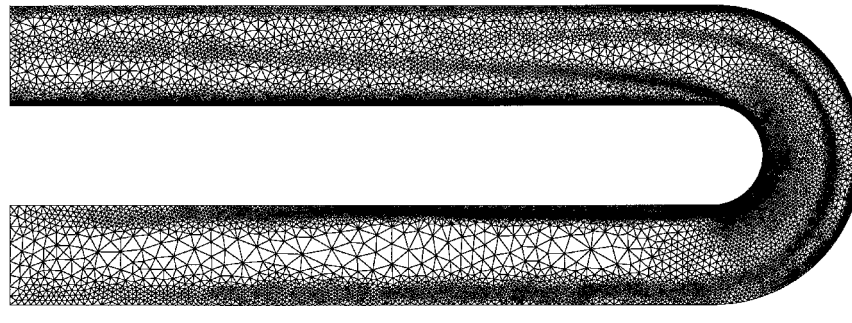

Fig. 2 Adaptive mesh 7 (72,831 nodes) for model 1 with $d = 0.01$.

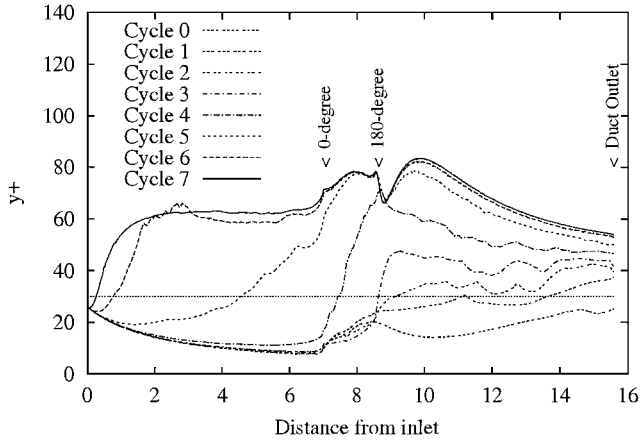

a) y^+

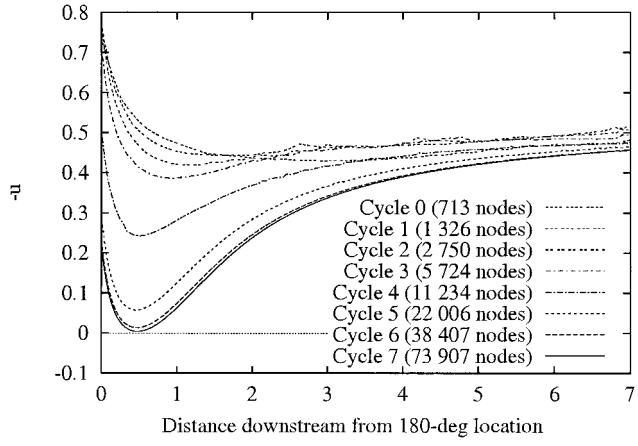

b) Slip velocity

Fig. 3 Slip velocity and y^+ along inner wall for model 1 with $d = 0.015$.

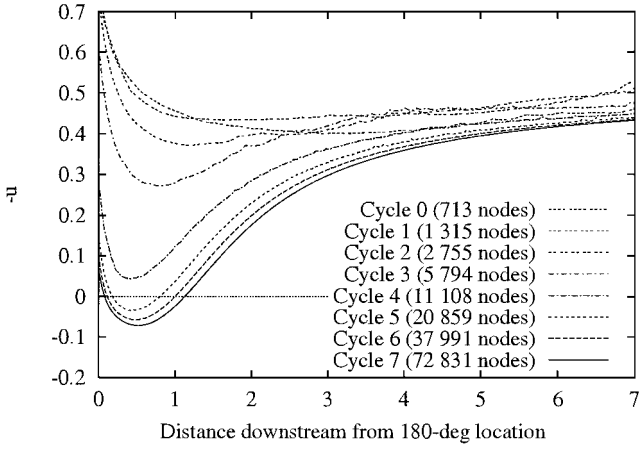

Fig. 4 Slip velocity along inner wall for $d = 0.01$ for computational model 1.

boundary. However, this time, the trend toward grid convergence of the results is not as obvious as for the case with $d = 0.015$. A finer adaptive mesh could not be run because of computer resource limitations. Nevertheless, cycles 4–7 indicate a trend toward grid convergence, albeit at a slower rate, which indicates that the asymptotic range is more difficult to reach. Notice that for this smaller value of the wall distance, separation is predicted, but only on the finer meshes. Thus, separation can be predicted if two conditions are met. First, the wall distance must be small enough. Second, the mesh must be fine enough to guarantee grid convergence of the boundary condition.

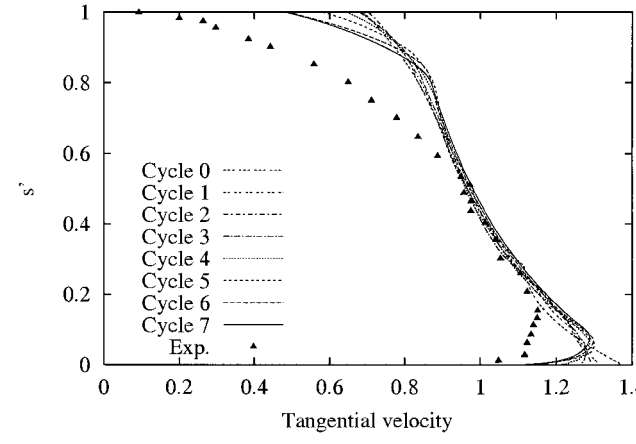

a) Location, 0 deg

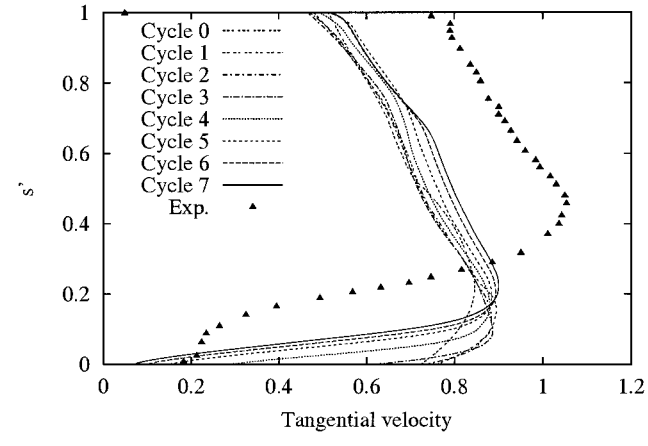

b) Location, 180 deg

Fig. 5 Streamwise velocity profiles for model 1 with $d = 0.01$ on inner wall.

Comparisons of the predicted and measured streamwise velocity component are shown in Fig. 5 for model 1 with $d = 0.01$. Note that the mesh exerts a fairly strong influence on the predictions. This is especially visible at the exit from the bend (180-deg location). The dimensionless coordinate s' is defined in the radial direction so that its value is zero at the inner wall and one on the outer wall. The numerical predictions are nearly grid converged on the finest mesh. However, the agreement with experiment is rather poor. These computations indicate that very fine meshes are required to ensure that nonlinear mixed boundary conditions provided by the wall functions are mesh converged. Hence, careful mesh refinement studies are required to guarantee reliable and verified predictions.

In their experiment, Sharma and Ostermier[15] observed that the flow in the upstream portion of the duct presented partially developed boundary layers occupying 40% of the duct height. Computational model 2 was designed to reflect this. The geometry is shown in Fig. 1. Boundary conditions for the TAD inlet were obtained by solving the developing flow in a straight section of the annular duct until the boundary layers reached the observed thickness. The distance d in the wall functions is set to 0.01 on the inner wall and 0.02 on the outer wall. Figure 6 presents the final mesh for computational model 2 obtained after seven cycles of grid adaptation. The evolution of the slip velocity with the mesh (Fig. 7) follows a pattern quite similar to that obtained with computational model 1 (Fig. 3b). Again, separation is predicted at the exit of the bend. The trend toward grid independence of the solution is confirmed by the slip velocity distributions for cycles 6 and 7 being nearly superimposed.

Predictions of streamwise velocity are compared with the measurements of Sharma and Ostermier[15] at various locations in the bend (at 0, 103, and 180 deg) in Fig. 8. We first verified the experimental flow rates obtained by integration of the measured velocity

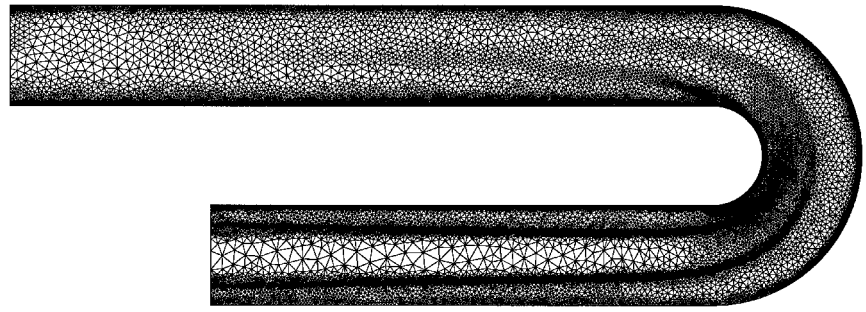

Fig. 6 Adaptive mesh 7 (96,522 nodes) for computational model 2.

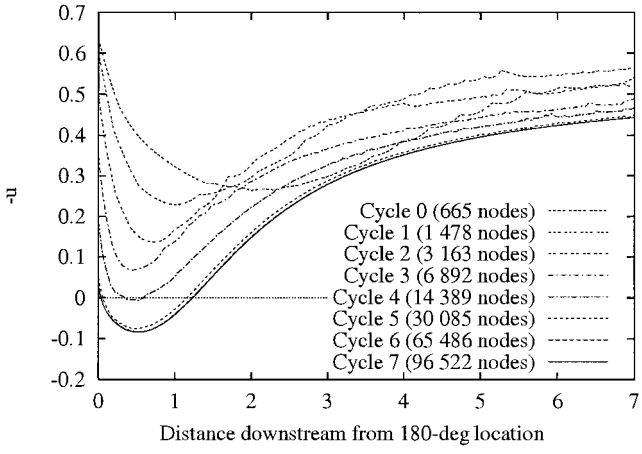

Fig. 7 Slip velocity along inner wall for computational model 2.

profiles at each station. These flow rates should be equal. Data show that they differ by as much as 12% from the nominal flow rate of 5140 ft^3/min (2.43 m^3/s) given by the present authors (see Ref. 15). The experimental data were mass adjusted to ensure that the mass flow rate was the same at each station. Hence, both sets of experimental data are reported. Grid-independent numerical predictions of the streamwise velocity obtained on cycle 7 with computational models 1 and 2 are presented in Fig. 8. The overall impression is that predictions obtained with model 2 are in better agreement with mass-adjusted experimental results than those obtained with model 1.

At the 103-deg locations (Fig. 8b), both models underestimate the velocity tangent to the outer and inner walls. At the 180 deg location (Fig. 8c), the main difference between the predictions of the two models is the location of the maximum velocity. Both models show incipient separation from inner wall ($s' = 0$). Although Sharma and Ostermier provide no details concerning the location and the length of the recirculation zone, they stated,

> There is definite indication that the flow has separated at the 180-degree measurement location. This occurs at the inner wall and is observed as an insignificant change in the velocity with distance from the inner wall. Since the hot-wire technique is unable to resolve recirculating flows, it is quite possible that the probe is in fact in its own probe-support-generated wake.[15]

The last statement certainly adds uncertainty to the accuracy of the experimental data. Assessment of uncertainties is the topic of the next section.

Sensitivities

We now turn our attention to sensitivity and uncertainty analysis using the apparently simpler problem of conjugate laminar free convection of corn syrup in an enclosure. This problem was studied experimentally and numerically by Chu and Hickox[5] as a model of convection in the Earth's mantle. This problem presents many

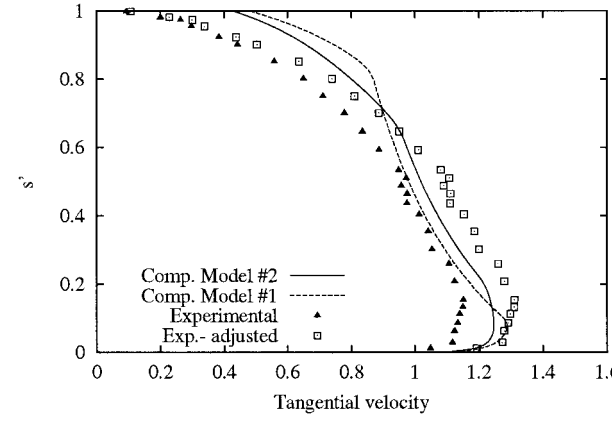

a) Location, 0 deg

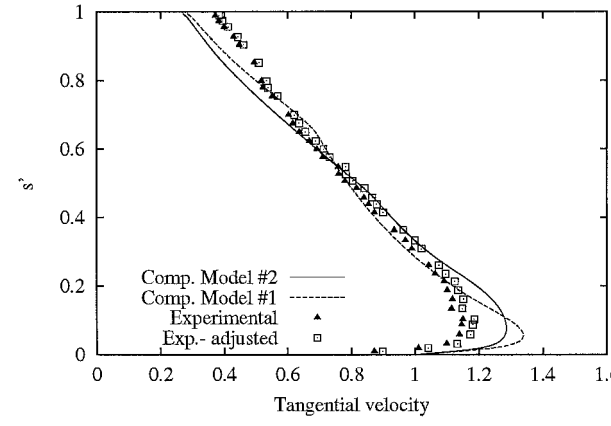

b) Location, 103 deg

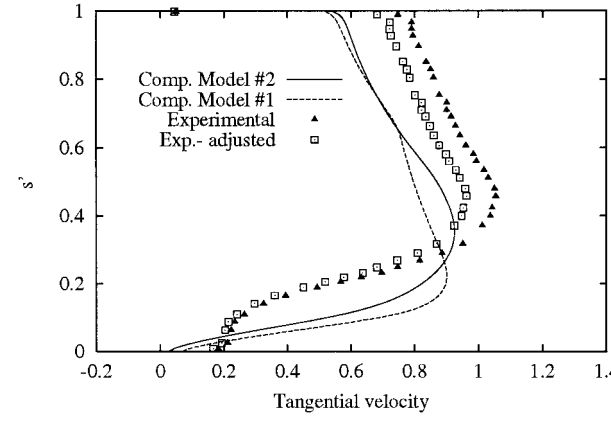

c) Location, 180 deg

Fig. 8 Experimental and predicted streamwise velocity profiles.

interesting features. First, the fluid properties are highly temperature dependent, leading to a complex dependence of the flow on several parameters. Secondly, uncertainties on several parameters were reported by the experimentalists, thus providing the data required to perform an uncertainty analysis. The focus is on application of the sensitivity equation method (SEM) to characterize the importance of the various parameters and to obtain uncertainty estimates of the CFD predictions. Mathematical and technical details of the SEM for this class of problems have been presented elsewhere. The interested reader is, thus, encouraged to consult the appropriate references.[16–18] These references also provide details about the finite element flow solver. Here, our discussion focuses on applications of the SEM in the context of good CFD practice.

Problem Description

The computational domain modeling the experiment of Chu and Hickox[5] is sketched in Fig. 9. The base of the enclosure is constructed of Plexiglas®, and heat is transmitted to the fluid through a copper heating element that we assume maintained at a fixed temperature T_h. The top surface of the enclosure is maintained at a fixed cooler temperature T_0. The remainder of the domain is insulated. The velocity of the fluid is zero on all walls and a symmetry boundary condition is imposed on the vertical edge above the copper block. The material properties of the fluid are assumed to satisfy the relationships[5]

$$\mu = a_0 \exp\left(a_1 e^{-T/a_2}\right)$$

$$\kappa = b_0 + b_1 T$$

$$c_p = c_0 + c_1 T + c_2 T^2 \tag{13}$$

The values of the coefficients in the preceding expressions are those given by Chu and Hickox.[5] (See also Turgeon et al.[16–18])

The problem is modeled with the continuity, momentum, and energy equations with the Boussinesq approximation:

$$\nabla \cdot \boldsymbol{u} = 0 \tag{14}$$

$$\rho \boldsymbol{u} \cdot \nabla \boldsymbol{u} = -\nabla p + \nabla \cdot [\mu(\nabla \boldsymbol{u} + (\nabla \boldsymbol{u})^T)] - \rho \boldsymbol{g} \beta (T - T_0) \tag{15}$$

$$\rho c_p \boldsymbol{u} \cdot \nabla T = \nabla \cdot (\kappa \nabla T) \tag{16}$$

where the flow variables $\boldsymbol{u}$, p, and T are the velocity, pressure, and temperature, respectively. The density ρ, viscosity μ, coefficient of thermal expansion β, specific heat at constant pressure c_p, and thermal conductivity κ are fluid properties that may, in general, depend on $\boldsymbol{u}$, p, and T. The gravitational vector is $\boldsymbol{g}$. In this case, the difficulty arises from the nonlinear temperature dependence of the viscosity, specific heat, and thermal conductivity. In the copper and Plexiglas, only the heat conduction equation is needed. The differential equations for the fluid and solid regions are solved in a fully coupled manner by the use of the same finite element method used for the turbulent flow of the preceding section. Details may be found in our previous work.[18]

We follow Chu and Hickox[5] and set $T_0 = 5.3°\text{C}$, $\Delta T = 51.9°\text{C}$, $\rho_0 = 1.4334 \times 10^3$ kg/m^3, and the length of the copper strip, $L = h = 0.136$ m. The half-width of the enclosure measures $2.06L$ and the thickness of the Plexiglas and copper plate are $0.1L$ and $0.02L$, respectively. The x axis lies on the syrup/copper interface, whereas the y axis coincides with the symmetry axis.

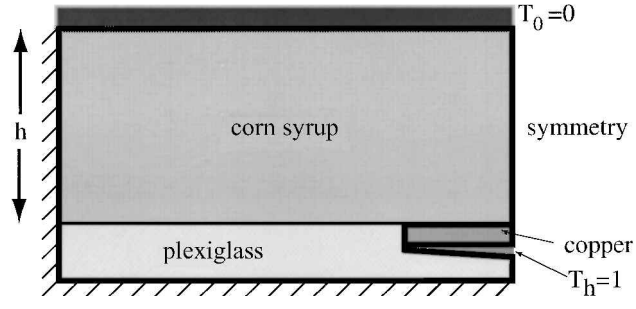

Fig. 9 Experimental setup of Chu and Hickox.[5]

For the conditions used by Chu and Hickox,[5] the Rayleigh and Prandtl numbers are

$$Pr_0 = \mu_0 c_{p0}/\kappa_0 \tag{17}$$

$$Ra_0 = \frac{\rho_0^2 c_{p0} \|\boldsymbol{g}\| \beta_0 \Delta T L^3}{\mu_0 \kappa_0} \tag{18}$$

whereas the ratio of viscosity is $\mu_0/\mu_h = 1026$.

Sensitivity Equations

The presence of several parameters tainted with uncertainty makes this problem a good subject for uncertainty analysis. We consider the following four parameters:

1) The viscosity model is accurate to within 6.5%. We choose the coefficient a_0 to absorb this uncertainty, that is, $a_0 \pm \Delta a_0$ with $\Delta a_0 = 0.065 a_0$.

2) The thermal conductivity model is accurate to 3%. We assign this uncertainty of the parameter b_0 to $\Delta b_0 = 0.03 b_0$.

3) Chu and Hickox[5] describe the enclosure height h as equal to the length of the heater. However, in their computation, they use $h = 0.98L$. Thus, we consider an uncertainty of $0.02L$ for this parameter.

4) The measured temperatures vary by as much as 2% over the central region of the heated strip, and so we take $\Delta T_h = 0.02(T_h - T_0)$.

As mentioned earlier, we consider only parametric uncertainties. For example, a_0 and T_h are assumed constant with an uncertain value. In a more realistic approach, the uncertainties may cause local perturbations: T_h will not be uniform, and the viscosity model may exhibit local deviations (depending on T) compared to the real fluid behavior. In some sense, we look at an extreme case.

We define the flow sensitivities as the partial derivatives of the flow solution with respect to parameter a: $\boldsymbol{s}_u = \partial \boldsymbol{u}/\partial a$, $s_p = \partial p/\partial a$, $s_T = \partial T/\partial a$. We denote the derivatives of the other coefficients by a prime. Following a general approach,[16] we differentiate Eqs. (14–16) with respect to a and obtain

$$\nabla \cdot \boldsymbol{s}_u = 0 \tag{19}$$

$$\rho' \boldsymbol{u} \cdot \nabla \boldsymbol{u} + \rho \boldsymbol{s}_u \cdot \nabla \boldsymbol{u} + \rho \boldsymbol{u} \cdot \nabla \boldsymbol{s}_u = -\nabla s_p \tag{20}$$

$$+ \nabla \cdot \left[\mu'(\nabla \boldsymbol{u} + (\nabla \boldsymbol{u})^T) + \mu\left(\nabla \boldsymbol{s}_u + (\nabla \boldsymbol{s}_u)^T\right)\right] \tag{21}$$

$$- (\rho' \boldsymbol{g} \beta + \rho \boldsymbol{g}' \beta + \rho \boldsymbol{g} \beta')(T - T_0) - \rho \boldsymbol{g} \beta (s_T - T_0') \tag{22}$$

$$(\rho' c_p + \rho c_p') \boldsymbol{u} \cdot \nabla T + \rho c_p (\boldsymbol{s}_u \cdot \nabla T + \boldsymbol{u} \cdot \nabla s_T)$$

$$= \nabla \cdot (\kappa' \nabla T + \kappa \nabla s_T) \tag{23}$$

If the material properties are variable, then their differentiation must account for the total functional dependence. For example, in the present case, we have

$$\mu = \mu(a, T) \tag{24}$$

then

$$\mu' = \frac{\partial \mu}{\partial a} + \frac{\partial \mu}{\partial T} s_T \tag{25}$$

If the function μ is known, then the necessary derivatives of μ are either known or can be approximated. Similarly, the sensitivities of the conductivity and specific heat are

$$\kappa' = \frac{\partial \kappa}{\partial a} + \frac{\partial \kappa}{\partial T} s_T \tag{26}$$

$$c_p' = \frac{\partial c_p}{\partial a} + \frac{\partial c_p}{\partial T} s_T \tag{27}$$

Boundary conditions for sensitivities are obtained in a similar manner by differentiation of the boundary conditions for the flow. See

Turgeon et al.[16,18] for details. For example, the boundary condition for the sensitivity of temperature $s_T = \partial T/\partial a$ is

$$s_T = -\nabla T \cdot \Pi_a + \frac{\mathrm{d}T_{\mathrm{bc}}}{\mathrm{d}a} \tag{28}$$

where $\Pi_a \equiv (\partial x_i/\partial a, \partial y_i/\partial a)$ is known along Γ_{d_i}. The term $\nabla T \cdot \Pi_a$ accounts for the displacement of the point of application of the boundary condition, whereas $\mathrm{d}T_{\mathrm{bc}}/\mathrm{d}a$ expresses the rate of change of the boundary condition value with respect to a. A similar strategy can be applied to find all of the sensitivity boundary conditions.

Uncertainty Analysis

Consider the temperature field T. Its distribution depends on some parameters $\boldsymbol{a} = (a_1, a_2, \ldots, a_n)$ describing geometry, boundary conditions, or fluid properties. If $\boldsymbol{a}$ is perturbed by $\Delta\boldsymbol{a}$, the temperature at a point (x, y) may be approximated by the use of a first-order Taylor series expansion:

$$T(x, y; \boldsymbol{a} + \Delta\boldsymbol{a}) - T(x, y; \boldsymbol{a}) = \sum_{i=1}^{n} \frac{\partial T}{\partial a_i}(x, y; \boldsymbol{a})\Delta a_i \tag{29}$$

We now seek how uncertainty propagates from $\boldsymbol{a}$ to T. We assume that $\Delta\boldsymbol{a}$ is the uncertainty on $\boldsymbol{a}$, that is, $\boldsymbol{a}$ lies somewhere in the interval $[\boldsymbol{a} \pm \Delta\boldsymbol{a}]$. Then the maximum possible change of T, that is, its uncertainty ΔT, is obtained when the components of $\boldsymbol{a}$ reach their maximum absolute values, so that they all push together in the same direction, increasing (or reducing) T. The uncertainty on T corresponds to the worst-case scenario, where temperature changes due to each disturbance Δa_i add up. Thus, we approximate the uncertainty on temperature by

$$|\Delta T| \approx \sum_{i=1}^{n} \left|\frac{\partial T}{\partial a_i}(x, y; \boldsymbol{a})\right| |\Delta a_i| \tag{30}$$

The preceding development is valid for a single parameter or a set of discrete parameters. Similar expressions hold for all flow variables.

Application

In the present analysis, we consider the following four parameters: the leading coefficient a_0 in the viscosity equation, the constant b_0 in the conductivity equation, the temperature of the heating element T_h, and the height h of the enclosure.

The Dirichlet boundary conditions for the sensitivities are 0 or 1 everywhere, except for the shape parameter h. In this case, $\Pi_a = (0, 1)$, so that $s_u = -\partial u/\partial y$ and $s_v = -\partial v/\partial y$ on the top boundary. In practice, we replace the preceding boundary condition on s_v by $s_v = 0$. This is equivalent and avoids problems with mass conservation.[17] Finally, on fixed boundaries, zero Neumann conditions for the flow become zero Neumann conditions for the sensitivities. The flow and sensitivities to the four aforementioned parameters are calculated by the use of an adaptive finite element method. Figures 10 illustrate the behavior of the flow: a thermal plume rising above the copper element and thermal boundary layers near the heated and cooled boundaries.

To illustrate the sensitivity solution, Fig. 11 presents graphs of the scaled sensitivities S_T^s which are defined as

$$S_T^s = \frac{\partial T}{\partial a} a_{\mathrm{nom}} \tag{31}$$

where a_{nom} is the nominal value of parameter a. Scaled sensitivities are a means of comparing the effect of parameters having wildly different magnitudes and units. Thus, for two parameters a and b, comparison of $(\partial T/\partial a)a_{\mathrm{nom}}$ with $(\partial T/\partial b)b_{\mathrm{nom}}$ is more meaningful because they have the same units. The comparison is also more meaningful because scaled sensitivities are related to perturbations of the system response due to relative perturbations of the parameters, instead of absolute perturbations.

Thus, if the scaled sensitivity for the parameter a is n times larger than the scaled sensitivity for the parameter b, then the temperature

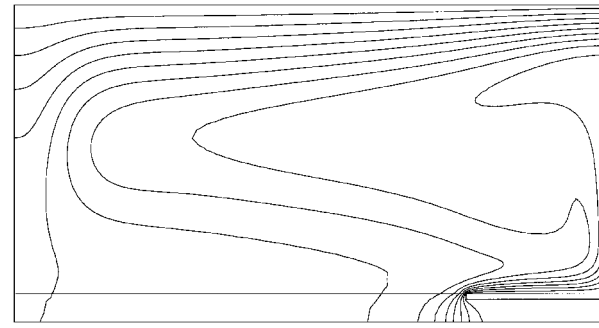

Fig. 10 Temperature contours.

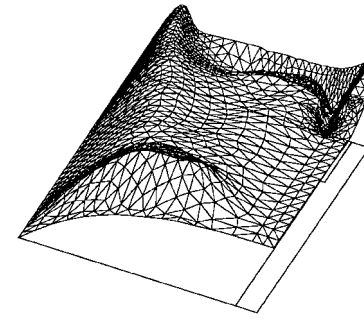

a) Parameter T_h

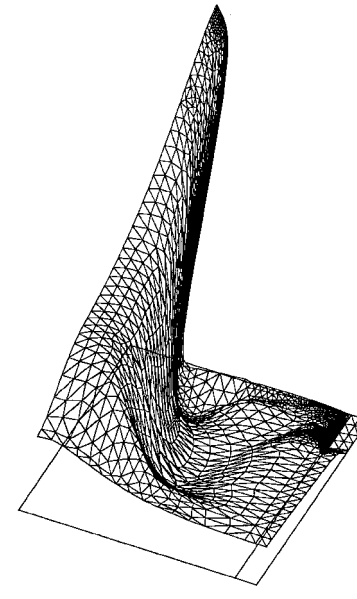

b) Parameter h

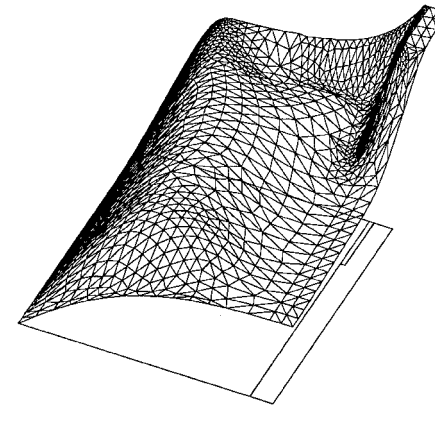

c) Flow solution T

Fig. 11 Scaled sensitivities of temperature.

change ΔT due to an $m\%$ perturbation of a will be n times larger than ΔT due to the same $m\%$ perturbation of b. The ratio of scaled sensitivities is the ratio of solution perturbations due to the same percent change in the parameters.

In the present example, $(\partial s_T/\partial b_0)b_0$ is the scaled sensitivity s_T for the parameter b_0. In Fig. 11, nodal values of the first adapted mesh are displaced vertically, according to the scaled sensitivity value. The temperature solution is also presented as a reference.

As can be seen, parameter h is highly dominant, at least in the upper region. Only this shape parameter provides a nonzero s_T on the top wall. Shape sensitivities on a parameter-dependent boundary are typically very large because a small displacement of the boundary produces large local perturbations. Near the copper plate, it is no surprise to observe that the temperature of the plate itself, T_h, has the strongest effect. Note that the temperature increases everywhere if T_h is increased (s_T is positive), whereas the sign of s_T varies within the domain for the other parameter. The distributions of the temperature and its sensitivities are very different. This is the reason why our remeshing strategy takes into account all variables (flow and sensitivities).

We can now use this sensitivity information to perform an uncertainty analysis. Figure 12 compares the numerical predictions and experimental measurements of the vertical velocity at $y = 0.4h$. The upper and lower bounds (dashed lines) on the flow predictions are computed using the first-order Taylor series expansion and account for uncertainties in the four parameters. In addition, the experimental measurements contain uncertainty. According to Chu and Hickox,[5] the velocity measurements are estimated to have an uncertainty of no more than 7%. We select this value for comparison purposes. Note that the uncertainty bands of numerical predictions and experimental measurements overlap. Thus, the agreement between predictions and measurements is very good. Velocity predictions are validated.

Similarly, Fig. 13 presents a comparison of the temperature distribution along the symmetry axis. Errors in the measurements of the temperature are difficult to assess, but a 0.7% value is often mentioned by Chu and Hickox. Once again, comparisons between predictions and experiments are based on uncertainty bands and not simply on predictions at the nominal values of the parameters. Again, overlap of the measured and predicted uncertainty intervals indicates good agreement and validation of the predictions.

The approach also yields uncertainty estimates for derived quantities such as the Nusselt number. We perform implicit differentiation of the definition of the Nusselt number:

$$Nu = \tilde{\kappa}\frac{\partial \tilde{T}}{\partial \tilde{y}} \tag{32}$$

to get

$$Nu' = \frac{\partial Nu}{\partial a_i}$$

$$Nu' = \tilde{\kappa}'\frac{\partial \tilde{T}}{\partial \tilde{y}} + \tilde{\kappa}\frac{\partial \tilde{s}_T}{\partial \tilde{y}} \tag{33}$$

so that the uncertainty estimate on Nu is given by

$$|\Delta Nu| = \sum_{i=1}^{4}\left|\frac{\partial Nu}{\partial a_i}\right||\Delta a_i| \tag{34}$$

Further details may be found in Ref. 18. Figure 14 shows the distribution of the Nusselt number along the hot copper plate with uncertainty bands. Over the copper surface, the Nusselt number behaves approximately like a thermal boundary layer: a peak near the edge of the copper element, followed by a regular decrease. The uncertainty is relatively uniform on the entire surface, except near the extremities of the heating element.

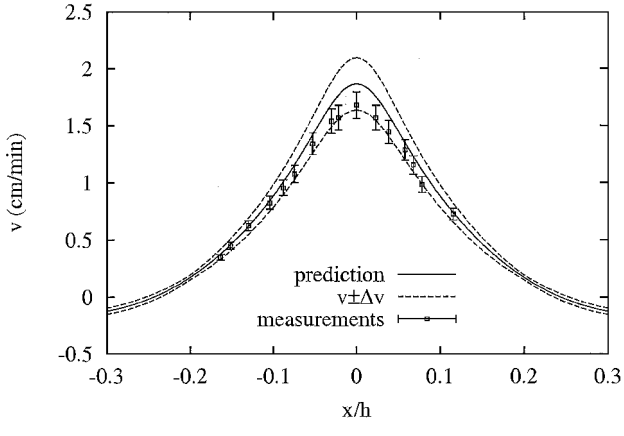

Fig. 12 Vertical velocity at $y = 0.4h$.

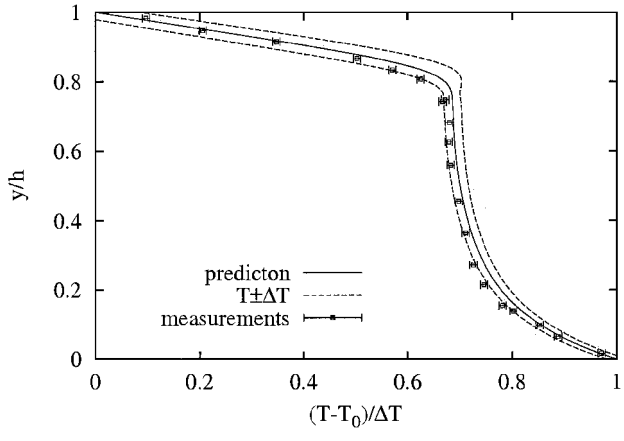

Fig. 13 Temperature distribution at $x = 0$.

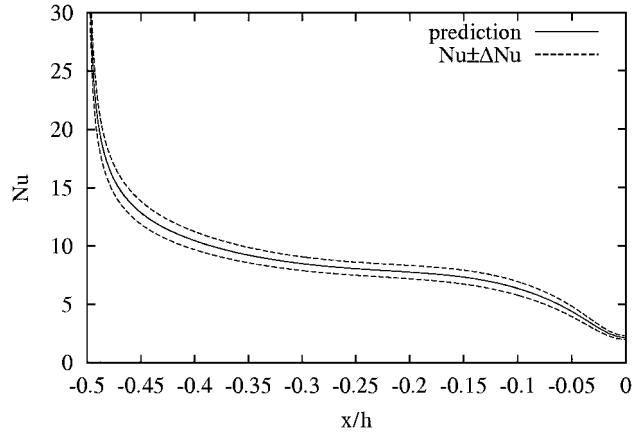

Fig. 14 Nusselt number along the copper plate.

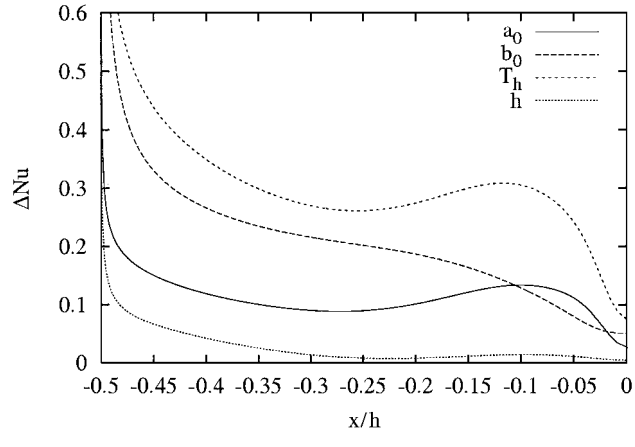

Fig. 15 Contributions to the uncertainty on Nusselt number.

Contributions from the four parameters to the uncertainty ΔNu along the copper plate are plotted in Fig. 15. The plate temperature T_h has the strongest effect, even if its 2% uncertainty is the smallest. Not surprisingly, conductivity has more influence on heat transfer than viscosity, even if the later has the largest uncertainty. Finally, the height of the enclosure has almost no effect for $x \in [-0.3, 0]$. Derivations of uncertainty estimates for the skin-friction coefficient and the location of the vortex center may be found in Ref. 18.

Conclusions

The combination of mesh adaptation and uncertainty analysis by the SEM is a powerful tool for verification and validation of CFD simulations. Although the methodologies were demonstrated on two-dimensional problems, it is believed that the following conclusions are valid in three dimensions.

Mesh adaptation is especially cost effective in that it automates the mesh refinement procedure. The analyst is, thus, relieved of a very tedious task and can focus his or her attention on ensuring that grid converged results are obtained before attempting comparison with measurements.

For turbulent flow, highly refined meshes are required to ensure grid-converged boundary conditions in wall functions. Results for two-equation models of turbulence in a turn-around duct show that flow predictions are very sensitive to the mesh size near the wall.

Sensitivity analysis is a powerful tool to characterize the dependence of the flow response on its input parameters. Sensitivity analysis provides information on which parameter has the most influence and where in the domain. This can be especially useful in design optimization because it offers the potential to reduce the number of design parameters.

Flow sensitivities are used to propagate model parameter uncertainties through a CFD code to yield uncertainty estimates of the CFD predictions. Uncertainty analysis of CFD results provides a rigorous framework for comparing predictions to measurements (validation of predictions). The resulting uncertainty bars put CFD on par with experimental techniques. Thus, comparison of predictions with measurements becomes a more rigorous and meaningful exercise.

Taken together, mesh adaptation, sensitivity analysis, and uncertainty analysis offer good prospects for developing families of computing methods that can be viewed as standards of good practice in CFD that ensure that verification and validation studies are performed on solid grounds.

Acknowledgments

This work was sponsored in part by NSERC (Natural Sciences and Engineering Research Council) (Government of Canada), Fonds Concerté d'Aide à la Recherche (FCAR) (Government of Québec), the Canada Research Chair Program, and the U.S. Air Force Office of Scientific Research (AFOSR) under Grant AFOSR F49620-00-1-0299.

References

[1]Nallasamy, M., "Turbulence Models and their Applications to the Predictions of Internal Flows," *Computers and Fluids*, Vol. 15, 1987, pp. 151–194.

[2]Roache, P., *Verification and Validation in Computational Science and Engineering*, Hermosa, Albuquerque, NM, 1998.

[3] "Guide for the Verfication and Validation of Computational Fluid Dynamics Simulations," TR AIAA-G-077-1998, June 1998.

[4]Oberkampf, W. L., Blottner, F. G., and Aeshliman, D., "Methodology for Computational Fluid Dynamics Code Verification and Validation," AIAA Paper 95-2226, June 1995.

[5]Chu, T. Y., and Hickox, C. E., "Thermal Convection with Large Viscosity Variations in an Enclosure with Localized Heating," *Journal of Heat Transfer*, Vol. 112, 1990, pp. 388–395.

[6]Launder, B. E., and Spalding, D. B., "The Numerical Computation of Turbulent Flows," *Computer Methods in Applied Mechanics and Engineering*, Vol. 3, 1974, pp. 269–289.

[7]Ilinca, F., and Pelletier, D., "Positiviy Preservation and Adaptive Solution of Two-Equation Models of Turbulence," *International Journal of Thermal Sciences*, Vol. 38, 1999, pp. 560–571.

[8]Kays, W., and Crawford, M., *Convective Heat and Mass Transfer*, 2nd ed., McGraw–Hill, New York, 1980.

[9]Schetz, J. A., *Boundary Layer Analysis*, Prentice–Hall, Upper Saddle River, NJ, 1993.

[10]Hughes, T. J. R., and Brooks, A. N., "A Multidimensional Upwind Scheme with No Crosswind Diffusion," *Finite Element Methods for Convection Dominated Flows*, edited by T. J. R. Hughes, Vol. 34, American Society of Mechanical Engineers, New York, 1979, pp. 19–35.

[11]Brooks, A. N., and Hughes, T. J. R., "Streamline Upwind/Petrov–Galerkin Formulations for Convection Dominated Flows with Particular Emphasis on the Incompressible Navier–Stokes Equations," *Computer Methods in Applied Mechanics and Engineering*, Vol. 32, 1982, pp. 199–259.

[12]Hughes, T. J. R., Franca, L. P., and Hulbert, G. M., "A New Finite Element Formulation for Computational Fluid Dynamics: VIII. The Galerkin/Least-Squares Method for Advective–Diffusive Equations," *Computer Methods in Applied Mechanics and Engineering*, Vol. 73, 1989, pp. 173–189.

[13]Crouzeix, M., and Raviart, P., "Conforming and Non-conforming Finite Element Methods for Solving the Stationary Stokes Equations," *Revue Française d'Automatique et de Recherche Opérationelle*, Vol. 3, 1973, pp. 77–104.

[14]Lacasse, D., Turgeon, É., and Pelletier, D., "Prediction of Turbulent Separated Flow in a Turnaround Duct Using Wall Functions and Adaptivity," AIAA Paper 2001-0448, Jan. 2001.

[15]Sharma, L. K., and Ostermier, B. J., "Flowfield Characteristics of an Axisymmetric 180-Degree Turnaround Duct," AIAA Paper 87-1357, June 1987.

[16]Turgeon, É., Pelletier, D., and Borggaard, J., "A General Continuous Sensitivity Equation Formulation for Complex Flows," AIAA Paper 2000-4732, Sept. 2000.

[17]Turgeon, É., Pelletier, D., and Borggaard, J., "A Continuous Sensitivity Equation Method for Flows with Temperature Dependent Properties," AIAA Paper 2000-4821, Sept. 2000.

[18]Turgeon, É., Pelletier, D., and Borggaard, J., "Sensitivity and Uncertainty Analysis for Variable Property Flows," AIAA Paper 2001-0140, Jan. 2001.

R. M. C. So
Associate Editor